Int. J. Electrochem. Sci., 13 **(2018)** 1515 – 1526, doi: 10.20964/2018.02.13

International Journal of
ELECTROCHEMICAL
SCIENCE
www.electrochemsci.org

Short Communication

Pitting Resistance of the Modified 13Cr Martensitic Stainless Steel in Chloride Solution

Moch. Syaiful Anwar[*], *Toni Bambang Romijarso, Efendi Mabruri*

Research Center for Metallurgy and Materials – Indonesian Institute of Sciences (LIPI)
Kawasan PUSPIPTEK Building 470 – Tangerang Selatan – Banten – 15314, Indonesia
[*]E-mail: moch026@lipi.go.id

Received: 19 July 2017 / *Accepted:* 28 September 2017 / *Published:* 28 December 2017

In this study, the influence of molybdenum (Mo) and nickel (Ni) on the pitting resistance of the 13Cr martensitic stainless steels was investigated. X-ray diffraction analysis was performed to analyze the phases formed in the steels. The corrosion studies of 13Cr steels were performed in the 3.5% NaCl solution by cyclic polarization and electrochemical impedance spectroscopy. The corrosion product was studied by SEM and EDX analysis. The results revealed that the addition of Mo and Ni improved the corrosion resistance of 13Cr martensitic stainless steel in the 3.5% NaCl solution.

Keywords: martensitic stainless steel, 13chromium, molybdenum, nickel, corrosion, pitting, chloride, polarization, SEM-EDS

1. INTRODUCTION

Pitting corrosion is a major problem that leads to the failure of turbine blade in steam power plants. Pitting corrosion occurs when the turbine blade is exposed in the steam flow containing chlorides from the boiler, and the steam flow later forms a condensate on the surface of the turbine blade, especially in the last stage, where the blades are under low pressure conditions [1-2]. Pitting corrosion can also cause the initiation of crack and subsequently fracture on the turbine blade, as well as decreasing the efficiency of a steam turbine [3-5]. Several studies aimed to minimize corrosion on the martensitic stainless steels, which are the standard blade material in the steam turbine, have been performed using the modification of the alloy and a heat treatment process [6-10]. Recently, alloy modification of martensitic stainless steel has been shown to be an appropriate choice for increasing the high temperature resistance and corrosion resistance in order to increase the life of the steam turbine blade. For instance, molybdenum (Mo) addition in the martensitic stainless steels improves the

corrosion resistance of stainless steels, and nickel (Ni) exerts a positive effect by decreasing the formation of δ-ferrite and improves toughness, as well as corrosion of martensitic stainless steels; the presence of boron (B) in the martensitic stainless steels has a beneficial effect on the wear properties and corrosion resistance of the alloy [11-13]. The mechanical and corrosion properties of martensitic stainless steels are improved somewhat by ranges of alloy composition. When the alloy composition is out of these ranges, the properties of the alloy decline because of the absence of the passive film on the surface, formation of δ-ferrite, decreased toughness and excessive precipitation [14]. Hence, the combination of more than two alloying elements in the martensitic stainless steel has attracted considerable attention from researchers. According to these studies in the literature, the improvement in the pitting resistance of martensitic stainless steel was revealed by the increasing content of Cr and the addition of Mo and Ni [15]. However, to the best of our knowledge, the presence of Mo content of more than 2.5 wt% in the martensitic stainless steel has not been studied and reported. Hence, the purpose of the present research is to investigate the pitting resistance of modified 13Cr martensitic stainless steel with the addition of 1 and 3 tr% of Mo, and 3 wt% of Ni using potentiodynamic and potentiostatic polarization and the impedance test method, and we compared this material's pitting resistance with that of non-modified 13Cr martensitic stainless steel.

2. EXPERIMENTAL PROCEDURE

2.1. Steels preparation

The ingots of 13Cr martensitic stainless steel with four different compositions were prepared in an electric induction furnace and cast in the mold with the dimensions of 5x5x10 cm. The four ingots were hot-forged at the initial temperature of 1398 K (1125°C) to achieve an ingot cross-section size of approximately 3x3 cm. The specimens of 1 cm in thickness were cut for chemical composition test using OES (optical emission spectrometer). The chemical compositions of the alloys are presented in Table 1.

Table 1. Chemical composition 13Cr martensitic stainless steel used in this study (%mass)

Type of Steel	C	S	P	Mn	Si	Cr	Mo	Ni	Fe
13Cr	0.14	0.003	0.002	0.98	0.32	13.60	0.02	0.29	Bal.
13Cr1Mo	0.13	0.003	0.002	0.94	0.31	13.13	0.80	0.29	Bal.
13Cr3Mo	0.13	0.005	0.002	0.87	0.24	12.85	2.52	0.28	Bal.
13Cr3Mo3Ni	0.10	0.005	0.002	0.61	0.24	12.73	2.52	2.93	Bal.

The other forged specimens were austenitized at 1273 K (1000°C) for 1 h and quenched in the oil. Next, austenitized steels were tempered at 898 K (625°C) for 1 h, which was followed by air cooling to room temperature.

2.2. Specimen preparation

Specimens with the surface area of 2.5 cm^2 were prepared for the polarization and impedance measurements from the heat treated specimens using a cutting machine and were polished with SiC paper with grit varying from 120 to 800. The measurement was conducted in the 3.5% sodium chloride solution at room temperature using a Gamry G750 system. The specimens, a graphite rod and a saturated calomel electrode (SCE), were used as the working, auxiliary and reference electrode, respectively. The specimens were allowed to corrode freely for 1 h in the solution prior to beginning the measurements. At the end of this period, the open circuit potential (E_{oc}) was recorded, and the measurements were started from the value of E_{oc}.

2.3. Testing

2.3.1. X-ray diffraction measurements

X-ray diffraction measurements were performed on the heat treated specimens using Cu Kα radiation. The continuous mode with 2θ ranging from 30 to 90° was applied to analyze the phase formed in the steels.

2.3.2. Electrochemical impedance spectroscopy measurement

The stability of the oxidation product and the corrosion rate during the polarization test was studied using electrochemical impedance spectroscopy (EIS) measurements. EIS was conducted on the specimens to determine the resistance of charge transfer (R_{ct}) and the constant phase elements (Y_o). The impedance was measured using a sinusoidal voltage signal of 10 mV applied over the frequency range from 100 kHz to 10 MHz using the Gamry G750 system. The impedance values were plotted in a Nyquist plot and were fitted using a simplex algorithm.

2.3.3. Cyclic polarization measurement

To determine the breakdown (E_b) and protection (E_{prot}) potentials, cyclic polarization was carried out in the potential range between −600 mV and 1200 mV from E_{oc} at the forward scan rate of 5 mV s^{-1} and reverse scan of 1.5 mV s^{-1} with the current density limit of 10 mA cm^{-2}. After reaching the peak current density, reverse polarization was performed to determine the susceptibility of pitting corrosion in the specimens.

2.3.4. Potentiostatic polarization measurement

The peak current density (i_{peak}) and the total time for meta-stable pitting events (t_{pit}) on the heat treated specimen were analyzed using potentiostatic polarization. The data were reconstructed from the cyclic polarization curve into a potentiostatic curve, where the current flowing due to the applied potential was plotted as a function of time.

At the end of polarization measurements, the corrosion rate of the specimens was calculated according to ASTM G 102.

2.3.5. SEM and EDX measurement

The appearance of pitting corrosion occurred on the specimens after the polarization measurement specimen was analyzed by SEM and EDX. The specimens were cleaned by ethanol to remove the dust. Next, the samples were mounted on the specimen holder. The specimen surfaces were examined to determine the shape of the pitting corrosion and precipitate elements in the pit hole.

3. RESULTS AND DISCUSSION

3.1. XRD analysis

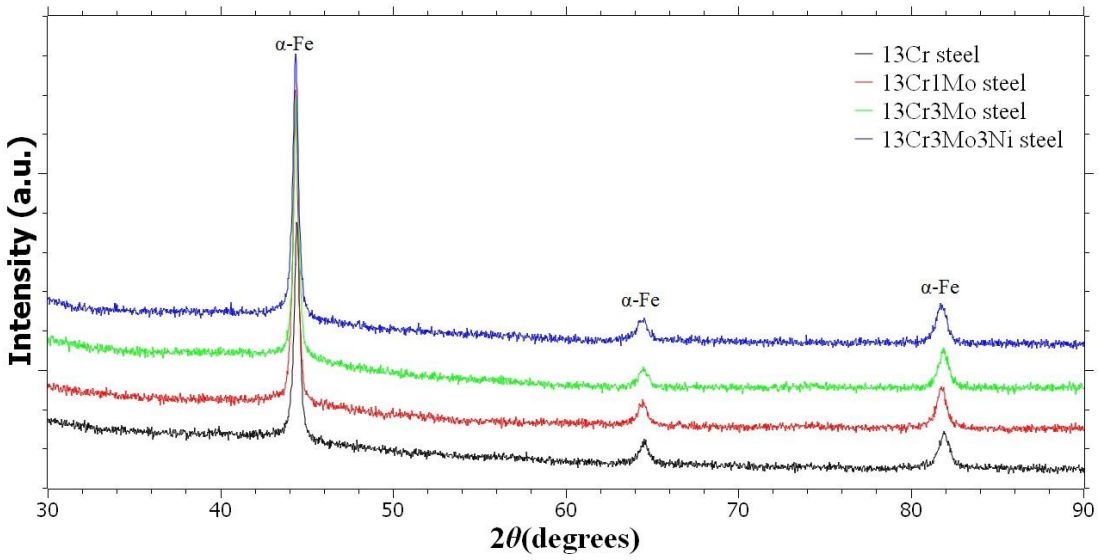

Figure 1. XRD analysis of the modified 13Cr martensitic stainless steel

The XRD results of the modified 13Cr martensitic stainless steel are shown in Figure 1. All heat-treated specimens of 13Cr martensitic stainless steel with and without Mo-Ni show only the α-Fe diffraction peak. The α-Fe peak is a signature of martensite or δ-ferrite contained in the steels. Similar results were obtained in the previous study that observed the 2θ values of the martensite diffraction peak to be approximately 45, 65 and 82.5 degrees [15]. By referring to the previous study, δ-ferrite

was observed by SEM in the martensitic stainless steels containing Mo, particularly in the 13Cr3Mo [16]. No γ-Fe peak was found among the XRD peaks, implying that all steel types contain very low levels of retained austenite [7].

3.2. EIS analysis

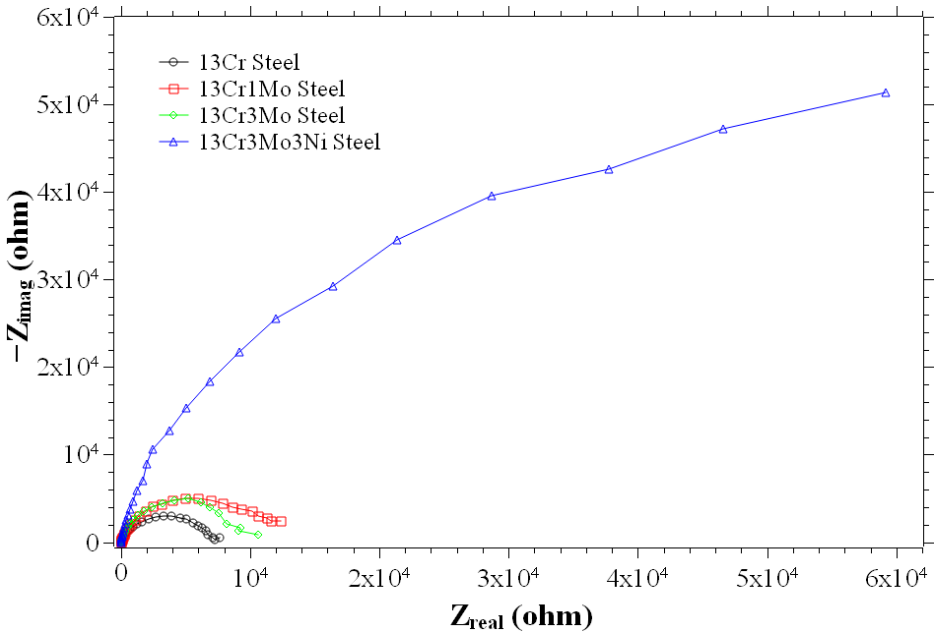

Figure 2. Nyquist plot of EIS for the modified 13Cr martensitic stainless steel in the 3.5% NaCl solution

The Nyquist plot of EIS for the 13Cr martensitic stainless steel with and without Mo and Ni in the 3.5% sodium chloride is presented in Figure 2.

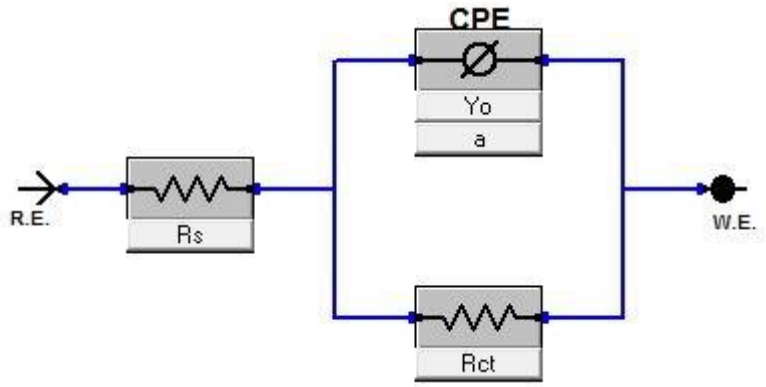

Figure 3. Equivalent circuit used for modeling the EIS result

The Nyquist plot of EIS shows that the curve of the semicircle occurs in the range of high frequency to low frequencies in all types of steel. This finding indicates that all types of steel have two

resistances, the solution resistance (Rs) and the charge transfer resistance (Rct). The best equivalent circuit used for modeling the Nyquist EIS plot is a simple Randall circuit model. In this model, a phase constant element (CPE) is used to analyze the behavior of the impedance electrical double layer accurately [17]. The equivalent circuit used for modeling the EIS result is shown in Figure 3. The simplex algorithm was used to fit the Nyquist EIS plot. The fitting results of EIS measurement are shown in Table 2.

Table 2. Result of EIS fit for the modified 13Cr martensitic stainless steel in the 3.5% NaCl solution

Type of Steel	R_{ct} (Ω cm^2)	CPE Y_o (μS cm^{-2} s^a)	A	Goodness of fit (%)
13Cr	18,701	77.5	0.86	0.15
13Cr1Mo	31,023	59.4	0.88	0.06
13Cr3Mo	26,392	46.5	0.90	0.16
13Cr3Mo3Ni	255,518	43.6	0.92	0.20

In Table 2, the R_{ct} value is the resistance of the passive layer of the steels. The CPE parameter defines the inhomogeneity of the surface in the electrochemical EIS experiments and the inhomogeneity of the charge distribution in solid-state EIS measurements. It is reasonable to expect that a better fit for real systems can be obtained using CPE [18]. The Yo value is an indication of the thickness of the passive layer. A lower Yo indicates the presence of a thicker passive layer and the 'a' value for all types of steel is less than 1, indicating that the passive layers formed on the steels are less capacitive [19].

The data in Table 2 indicated that the addition of Mo and Ni in the 13Cr martensitic stainless steel increases the R_{ct} value and decreases the Y_o value. Conversely, the 13Cr3Mo steel has the lowest R_{ct} and Y_o values among all steel types. This finding may indicate that the decrease of Rct is due to the presence of δ-ferrite in the 13Cr3Mo steel [14]. The highest R_{ct} value of 255,518 Ω cm^2 and the lowest Y_o value of 43.6 μS cm^{-2} s^a are observed in the 13Cr3Mo3Ni steel. This finding means that this steel exhibits the highest impedance for uniform corrosion.

3.3. Cyclic polarization analysis

The cyclic polarization data for 13Cr martensitic stainless steel with and without Mo and Ni in the 3.5% sodium chloride are presented in Figure 4.

The breakdown potential (E_b) is determined at the inflection point value above the sharp change in slope [20]. The protection potential (E_{prot}) is determined as a crossover potential. Cross-over potentials were measured for the closed hysteresis loops [21]. All types of 13Cr steel show hysteresis loops of pitting in the cyclic polarization curve.

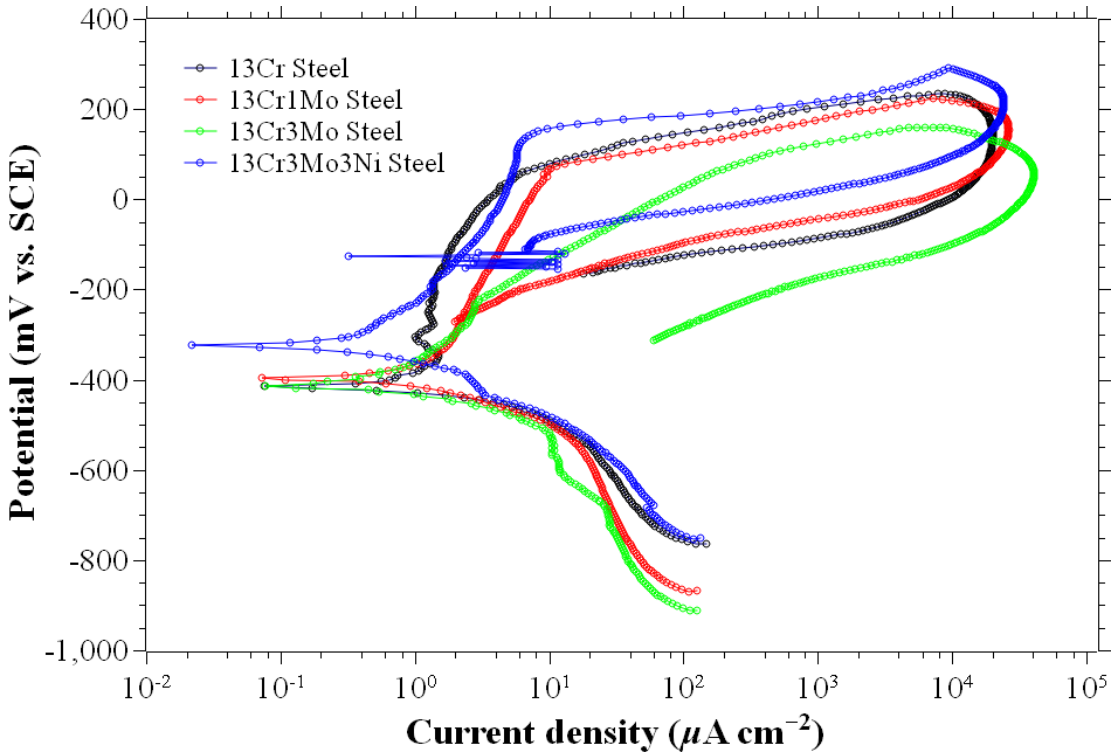

Figure 4. Cyclic polarization for the modified 13Cr martensitic stainless steel in the 3.5% NaCl solution

Table 3. Breakdown (E_b) and protection (E_{prot}) potential for the modified 13Cr martensitic stainless steel in the 3.5% NaCl solution

Steel	Breakdown potential, (E_b) (mV vs. SCE)	Protection potential, (E_{prot}) (mV vs. SCE)
13Cr	57.34	-165.9
13Cr1Mo	77.57	-261.4
13Cr3Mo	-228.6	-312.9
13Cr3Mo3Ni	153.5	-123.8

This finding indicates that pitting corrosion occurred on the surfaces of all types of steel after the cyclic polarization test.

Table 3 shows the E_b and E_{prot} values for each type of steel. As seen from the data presented in the table, E_b decreases significantly when 3 mass% of Mo is added to 13Cr steel. This finding may be due to the presence of δ-ferrite in the 13Cr3Mo steel [14]. The highest breakdown potential of 153.5 mV vs. SCE is exhibited by the 13Cr3Mo3Ni steel. This result means that the 13Cr3Mo3Ni steel has the highest resistance to pitting corrosion in the chloride environment among all steels [22].

3.4. Potentiostatic polarization analysis

The parameters of potentiostatic polarization are defined used the data presented in Figure 5. Peak current density (i_{peak}) is defined as, $i_{peak} = i_{max} - i_{bc}$. The total time for a meta-stable pitting event is given by $t_{pit} = t_g + t_{rp}$. In this equation, i_{max}: is the maximum current density, i_{bc} is the base current density, t_g is the pit growth time and t_{rp} is the repassivation time [23].

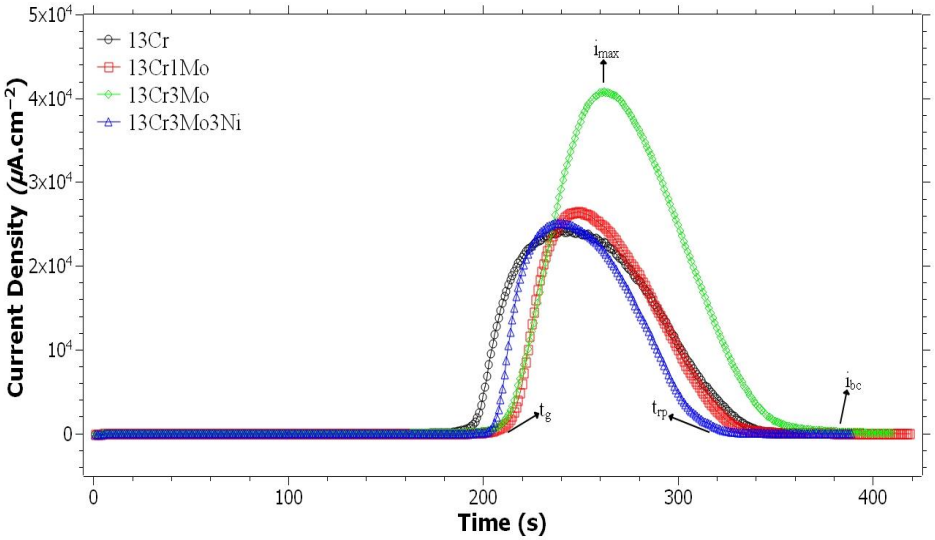

Figure 5. Potentiostatic polarization for the modified 13Cr martensitic stainless steel in the 3.5% NaCl solution

The potentiostatic polarization data for the modified 13Cr martensitic stainless steel in the 3.5% sodium chloride are presented in Figure 5. The current density of each type of steel shows a constant value until approximately 200 seconds, and the current density subsequently reaches the peak at approximately $3x10^4$ to $4x10^4$ $\mu A\ cm^{-2}$.

Table 4. Parameters determined from potentiostatic polarization for the modified 13Cr martensitic stainless steel in the 3.5% NaCl solution

Steel	i_{max} ($\mu A\ cm^{-2}$)	i_{bc} ($\mu A\ cm^{-2}$)	i_{peak} ($\mu A\ cm^{-2}$)	t_g (s)	t_{rep} (s)	t_{pit} (s)
13Cr	24,200	28	24,172	187	351	538
13Cr1Mo	26,510	7	26,503	206	340	546
13Cr3Mo	40,810	133	40,677	206	353	559
13Cr3Mo3Ni	25,100	12	25,088	203	329	532

Table 4 shows the values of the parameters determined from potentiostatic polarization for the modified 13Cr martensitic stainless steel in the 3.5% sodium chloride. The increase of Mo content in the 13Cr steel increases the peak current density (i_{peak}) value and the total time for a metastable pitting

event (t_{pit}). The highest peak current density of 40,677 μA cm^{-2} and total time for a metastable pitting event of 559 s are obtained for the 13Cr3Mo steel. This finding may indicate that the addition of 3 mass% Mo into the 13Cr martensitic stainless steel increases the susceptibility of steel to pitting corrosion in chloride environment. When the 3%Mo and 3% Ni by mass are added in 13Cr martensitic stainless steel, the values of i_{peak} and t_{pit} are lower than those of the steel without Mo. This finding is probably attributable to the positive effect of the Ni element for the resistance of the stable of δ-ferrite in this steel, which decreases the susceptibility of pitting corrosion in this steel [14].

3.5. Corrosion parameters of the modified 13Cr martensitic stainless steels

Table 5. Corrosion parameters of the modified the 13Cr martensitic stainless steels in the 3.5% NaCl solution

Steel	β_a* (mV/decade)	β_c* (mV/decade)	B (mV)	R_{ct}** ($\Omega.cm^2$)	i_{corr} ($\mu A.cm^{-2}$)	Eq. weight	Corrosion rate (mmpy)
13Cr	6988	91	39.01	18701	2.09	25.78	0.0226
13Cr1Mo	5571	136.5	57.85	31023	1.86	25.96	0.0204
13Cr3Mo	244.4	60.8	21.14	26392	0.80	25.85	0.0087
13Cr3Mo3Ni	298.7	72	25.19	255518	0.10	26.02	0.0011

Note: * Tafel data,
** EIS data

Table 5 shows the corrosion parameters of each type of steel calculated according to ASTM G 102. The density of 13Cr steels is 7.78 g cm^{-3}, β_a and β_b are obtained from the Tafel fit of the cyclic polarization and the R_{ct} value is obtained from the simplex fit of the EIS Nyquist plot.

The addition of Mo and Ni in the 13Cr steel reduces the βa and βc values. This finding indicates that the presence of Mo and Ni reduces the corrosion at the anodic and cathodic sites. The 13Cr1Mo steel shows the highest βc value. Hence, the 13Cr1Mo steel exhibits a higher corrosion rate than the 13Cr3Mo steel. The lowest corrosion rate of 0.0011 mmpy is found for the 13Cr3Mo3Ni martensitic stainless steel. Thus, the combination of 3%Mo and 3%Ni by mass added in the 13Cr steel shows the highest resistance to the uniform and pitting corrosion among all types of steel. By contrast, the 13Cr3Mo steel shows better resistance to the uniform corrosion but exhibits the worst resistance to pitting corrosion.

3.6. SEM and EDS analysis

SEM images of the 13Cr steel with and without Mo and Ni after the cyclic polarization test are compared in Figures 7a-d. The comparison clearly indicates that the surfaces of all types of steel suffer pitting corrosion (Figure 2). The addition of Mo and Ni in 13Cr steel reduces the diameter of the irregularly shaped pit.

Compared to Figure 5 and Table 4, the 13Cr3Mo steel in Figure 6c shows an irregular shape with smaller pit diameter than that of all steel types, but it shows a higher peak current density (Figure 5 and Table 4). This indicates that the 13Cr3Mo steel has the deepest pit among all types of steel.

Table 6. Partial EDS analysis inside the pit for the 13Cr steel with and without Mo and Ni after cyclic polarization test

Steel	Element (mass %)				
	Fe	Cr	C	O	Mo
13Cr	73.64	16.40	7.47	2.49	-
13Cr1Mo	79.10	18.67	-	1.39	0.84
13Cr3Mo	75.35	24.09	-	-	0.55
13Cr3Mo3Ni	67.51	13.76	14.49	4.24	-

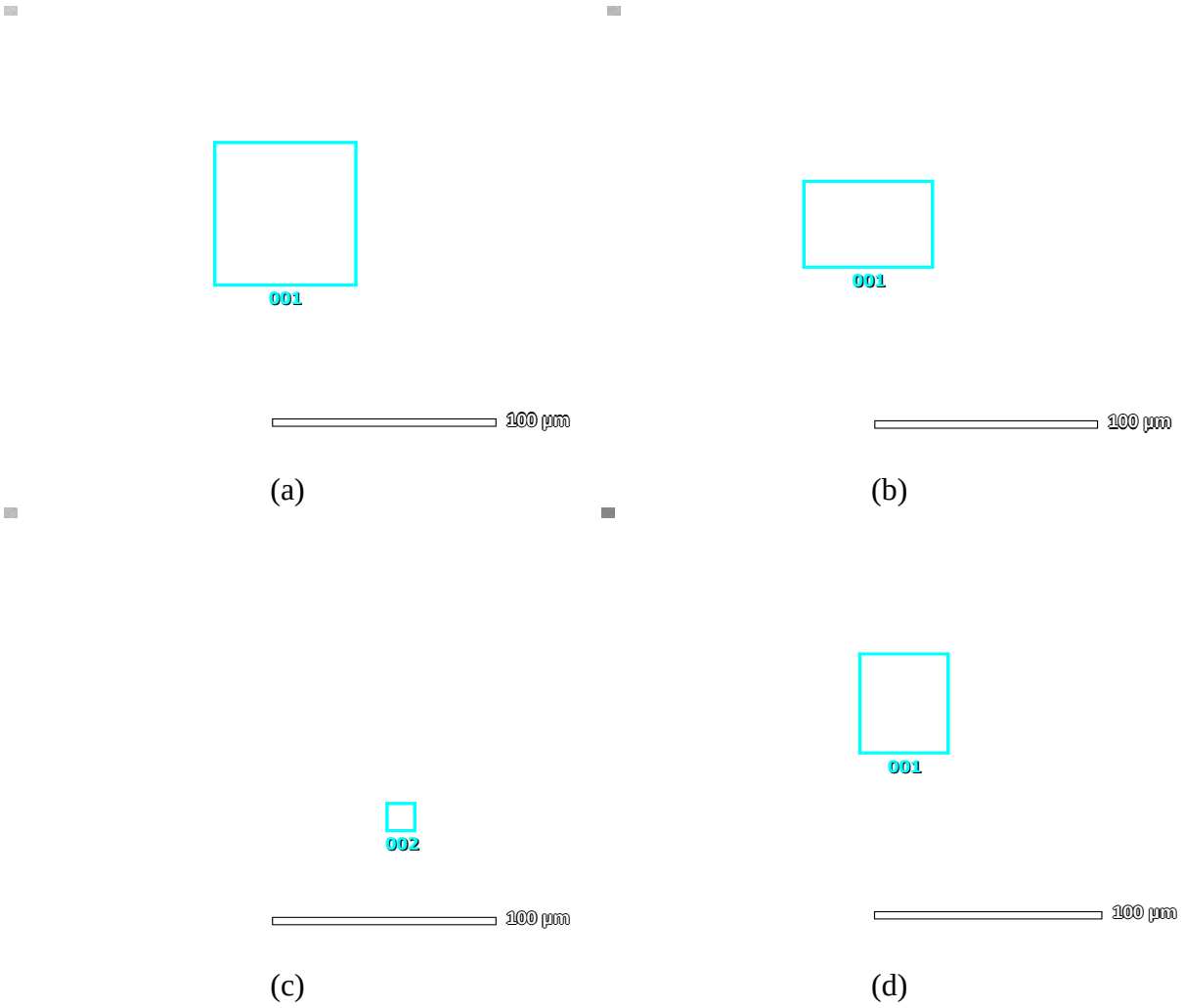

Figure 6. SEM image of (a) 13Cr steel, (b) 13Cr1Mo steel, (c) 13Cr3Mo steel and (d) 13Cr3Mo3Ni steel after cyclic polarization test with magnification 500x

Table 6 shows the results of a partial EDS analysis in the pit corrosion section for all types of steel. The carbon content of 7.47 mass% in the 13Cr steel and 14.49 mass% in the 13Cr3Mo3Ni steel

may indicate the availability of metal carbide precipitation in the pits. The precipitation of metal carbide in these steels has also been observed in a previous investigation [24]. However, the 13Cr1Mo steel and 13Cr3Mo steel show no carbon inside the pit. This finding indicates that there was very little precipitated metal carbide in the pits. Thus, the metal carbide that forms in the martensitic stainless steel does not have a direct effect on the occurrence of pitting corrosion.

The presence of oxygen contributes to the passive oxide layer formation on the surface of the steel. The higher oxygen content of 4.24% by mass is found on the 13Cr3Mo3Ni steel. This may indicate that the 13Cr3Mo3Ni steel has the highest breakdown potential among all types of steel. The absence of oxygen in the pit of the 13Cr3Mo steel indicates little passive film formation on the surface of this steel. This property may enable the more aggressive ions (Cl^-) to form pitting corrosion on the surface of this steel.

4. CONCLUSIONS

The molybdenum and nickel elements added in the 13Cr martensitic stainless steel decreased the corrosion rate in the 3.5% sodium chloride solution. The 13Cr steel with and without Mo and Ni still shows a susceptibility to the pitting corrosion in the 3.5% sodium chloride solution. The increase of 3 mass% Mo in the 13Cr steel has no effect on the breakdown potential (Eb) and even gives rise to the deepest pit. The best corrosion resistances were exhibited by the 13Cr3Mo3Ni martensitic stainless steels.

ACKNOWLEDGMENTS
This research was supported by the Program of Excellence of the Indonesian Institute of Sciences (LIPI), Fiscal Year 2016.

References

1. O. Jonas, L. Machemer, Steam Turbine Corrosion and Deposits Problems and Solutions, *Proceeding of The Thirty-Seventh Turbomachinery Symposium*, Texas, 2008, 211.
2. J. Wei, B. Zhou, *Int. J. Electrochem. Sci.*, 12 (2017) 3166.
3. T.H. McCloskey, Troubleshooting Turbine Steam Path Damage Mechanisms, *Proceeding of The Thirty-First Turbomachinery Symposium*, Texas, 2002, 105.
4. B.M. Schönbauer, A. Perlega, S.E. Stanzl-Tschegg, Pit-To-Crack Transition and Corrosion Fatigue of 12%Cr Steam Turbine Blade Steel, *13th International Conference on Fracture*, Beijing, China, 2013, 1.
5. E. Plesiutschnig, P. Fritzl, N. Enzinger, C. Sommitsch, *Case Stud. Eng. Fail. Anal.*, 5–6 (2016) 39.
6. Si-Yuan Lu, Ke-Fu Yao, Yun-Bo Chen, Miao-Hui Wang, Xue Liu, Xueyuan Ge, *Electrochim. Acta*, 165 (2015) 45.
7. T. Honda, E. C. Santos, K. Kida and T. Shibukawa. *Adv. Mater. Res.*, 457-458 (2012) 525.
8. A. N. Isfahany, H. Saghafian, G. Borhani. *J. Alloys Compd.*, 509 (2011) 3931.
9. Li-Bin Niu, H. Kato, K. Shiokawa, K. Nakamura, M. Yamashita, Y. Sakai, *Mater. Trans.*, 54 (2013) 2225.
10. E. Mabruri, Z. A. Syahlan, Sahlan, M. S. Anwar, T. B. Romijarso, B. Adjiantoro, *Int. J. Eng. Technol.*, 8 (2016) 2547.

11. G. Zepon, R. P. Nogueira, C. S. Kiminami, W. J. Botta, and C. Bolfarini, *Metall. Mater. Trans. A.*, 48 (2017) 2077.
12. E. Mabruri, M. S. Anwar, S. Prifiharni, T. B. Romijarso, B. Adjiantoro, Tensile Properties of the Modified 13Cr Martensitic Stainless Steels, *AIP Conference Proceeding*, 2015, 020039-1.
13. A. P. I. Popoola, O. S. Fatoba, O. M. Popoola, S. L. Pityana, *Silicon*, 8 (2016) 579.
14. S. Oikawa, H. Yoda, M. Arai, H. Doi, Precipitation hardening martensitic stainless steel, and steam turbine long blade, steam turbine, and power plant using the same, *Patent US9388702 B2*, 2016, US 13/741, 946.
15. X. Lei, Y. Feng, J. Zhang, A. Fu, C. Yin, D. D. Macdonald, *Electrochim. Acta*, 191 (2016) 640.
16. E. Mabruri, M. S. Anwar, S. Prifiharni, T. B. Romijarso, B. Adjiantoro, *Metalurgi*, 30 (3) (2015) 133.
17. N. Ebrahimi, M. Momeni, A. Kosari, M. Zakeri, M.H. Moayed. Corros. Sci., 59 (2012) 96.
18. J. R. Macdonald. Impedance Spectroscopy Emphasizing Solid Materials and Systems, *Electrochim. Acta*, 33 (1988) 725.
19. B. Hirschorn, M.E. Orazem, B. Tribollet, V. Vivier, I. Frateur, M. Musiani. *Electrochim. Acta*, 55 (2010) 6218.
20. G. S. Frankel. ASM Handbook , vol. 13A, ASM International, Metals Park, (2003) OH, USA.
21. R. Baboian and G. S. Haynes. STP 727 Electrochemical Corrosion Testing, ASTM, (1981) Philadelphia, PA, USA.
22. M. C. S. Fernandes, S. Nakamatsu, A. L. P. Rueda, J. J. Souza, S. C. D. Rezende, L. L. Souza, N. A. Mariano, *Mater. Res.*, (2017) 1, https://dx.doi.org/10.1590/1980-5373-mr-2016-1004.
23. R.K. Guptaa, N.L. Sukiman, M.K. Cavanaugh, B.R.W. Hinton, C.R. Hutchinson, and N. Birbili, *Electrochim. Acta*, 66 (2012) 245.
24. M. W. A. Rashid, M. Gakim, Z. M. Rosli, M. A.Azam. *Int. J. Electrochem. Sci.*, 7 (2012) 9465